Detecting temporal velocity changes using various methods

Haijiang Zhang

University of Science and Technology of China

Outline

- Seismic tomography between different time periods
- Repeating earthquakes
- Coda wave interferometry
- Ambient noise

Time-Resolved Seismic Tomography Detects Magma Intrusions at Mount Etna

D. Patanè *et al.*

Science **313**, 821 (2006);
DOI: 10.1126/science.1127724

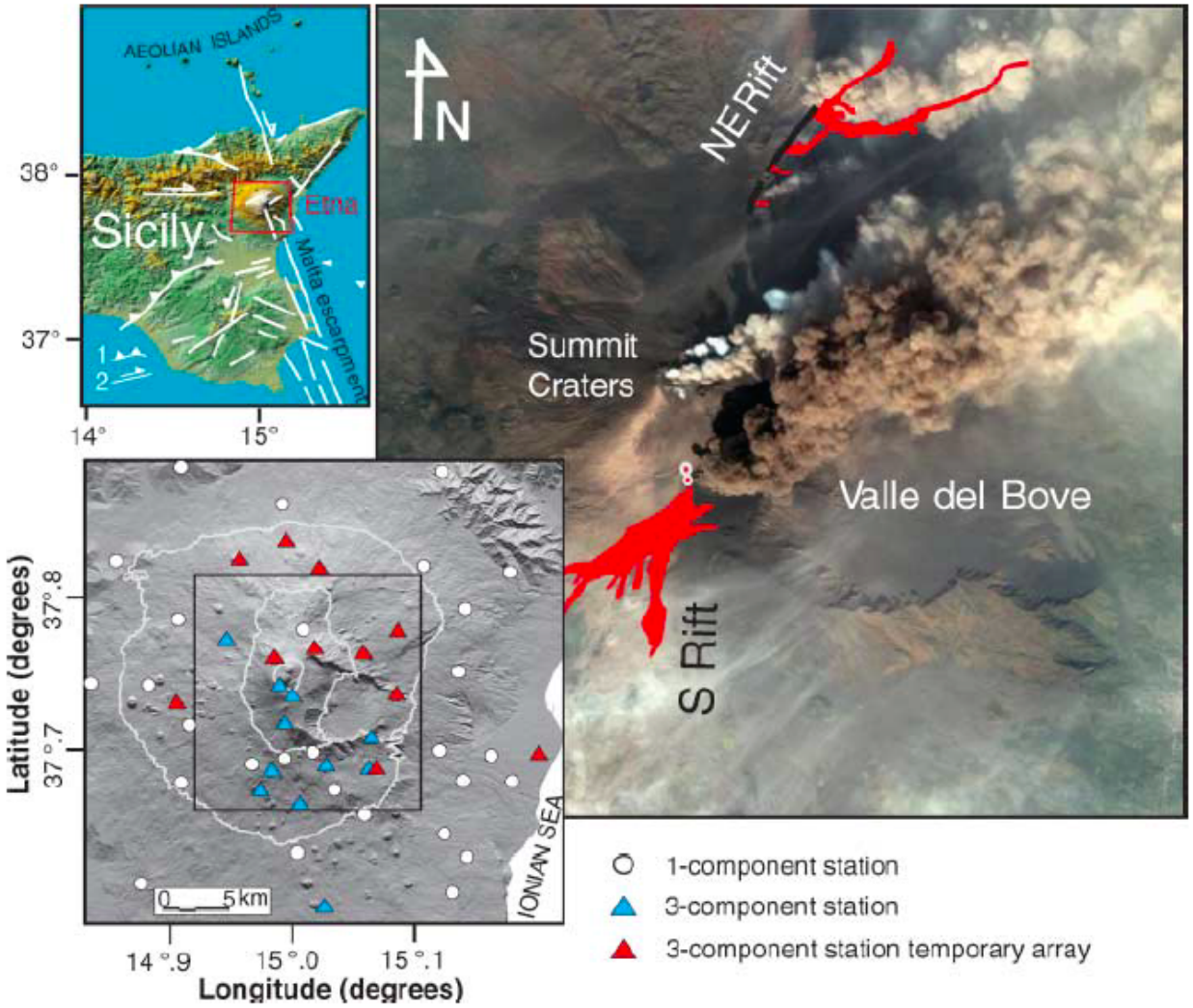

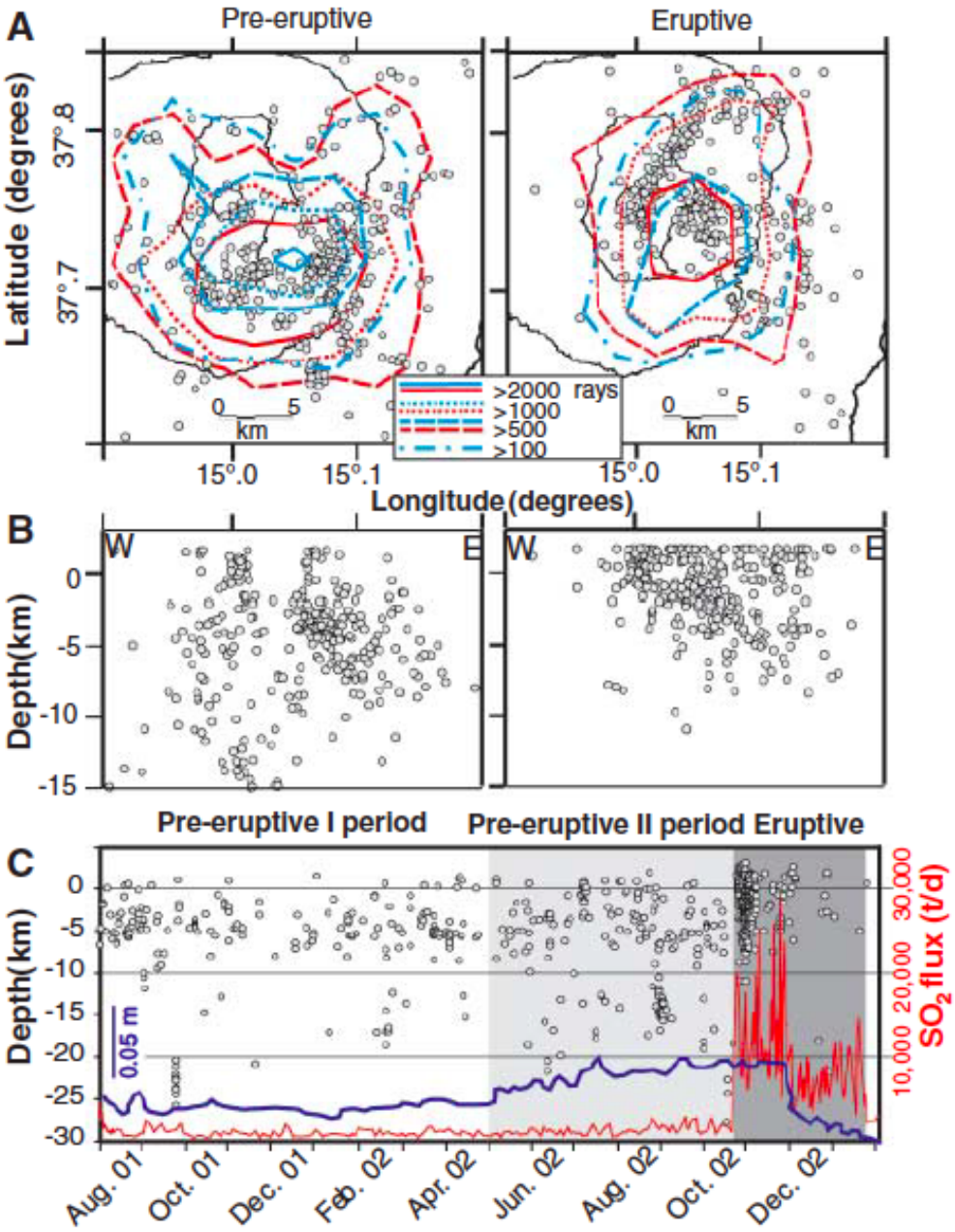
A
Pre-eruptive
Eruptive
Latitude (degrees)
37°.8
37°.7
0 5
km
>2000 rays
>1000
>500
>100
15°.0
15°.1
Longitude (degrees)
B
W
E
Depth(km)
0
-5
-10
-15
Pre-eruptive I period
Pre-eruptive II period
Eruptive
C
0.05 m
-20
-25
-30
10,000
20,000
30,000
SO2 flux (t/d)
Aug. 01
Oct. 01
Dec. 01
Feb. 02
Apr. 02
Jun. 02
Aug. 02
Oct. 02
Dec. 02

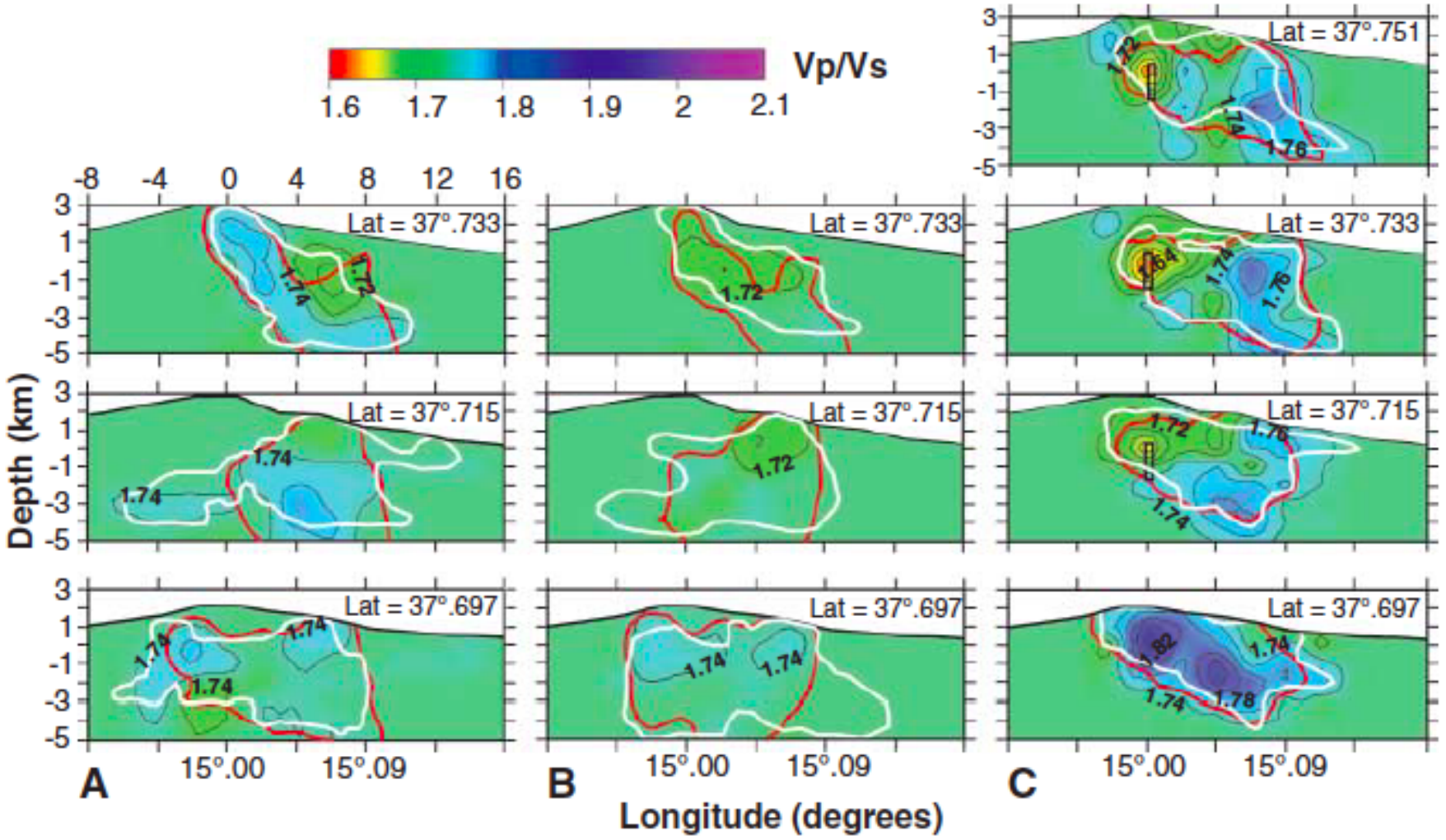

Fig. 4. W-E cross sections showing the variation of the V_P/V_S ratio during the pre-eruptive periods [(**A**) and (**B**)] and the 2002–2003 eruption (**C**). The vertical black rectangle in (C) indicates the location of the 2002–2003 dike intrusion, as modeled by geodetic data in the southern flank (*19*, *20*). The white and red lines indicate the well-resolved regions of the model with SF values <2 and derivative weight sum values >50, respectively (SOM text).

Different ray distribution on velocity models

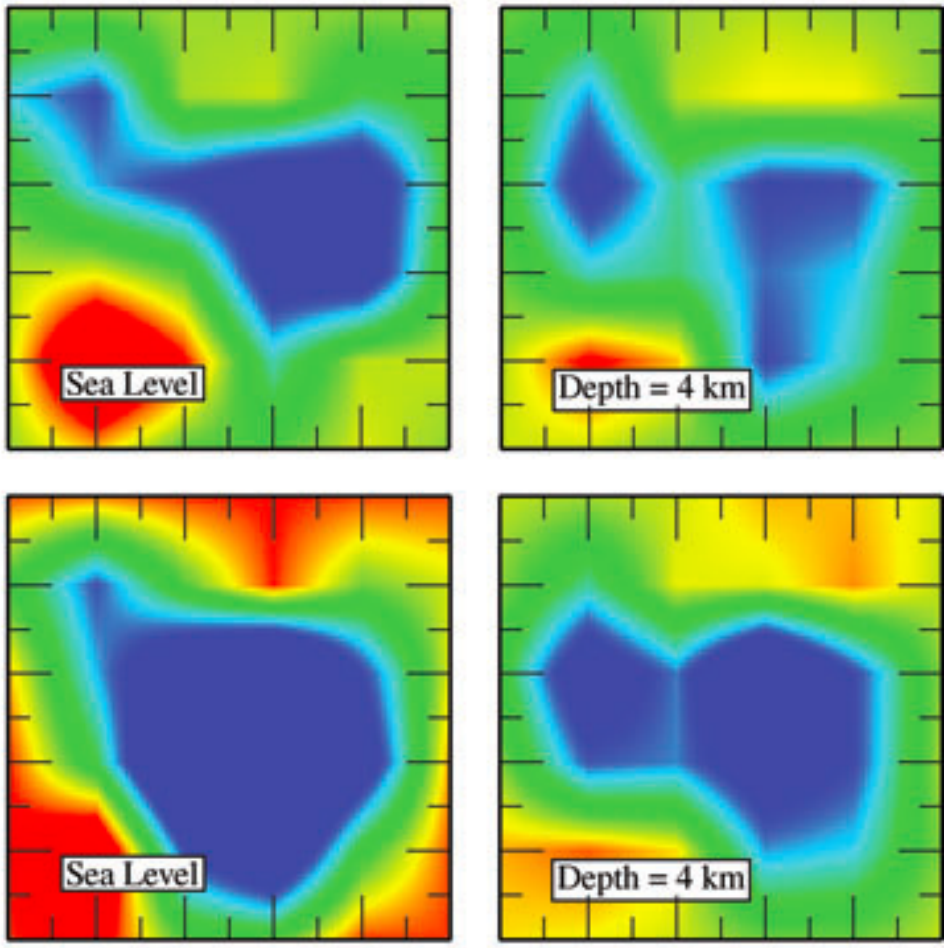

- Same theoretical models but with different ray distribution.
- Separately Inverted models are different

Time-dependent seismic tomography

B. R. Julian[1] and G. R. Foulger[2]

Different ray distribution on velocity models

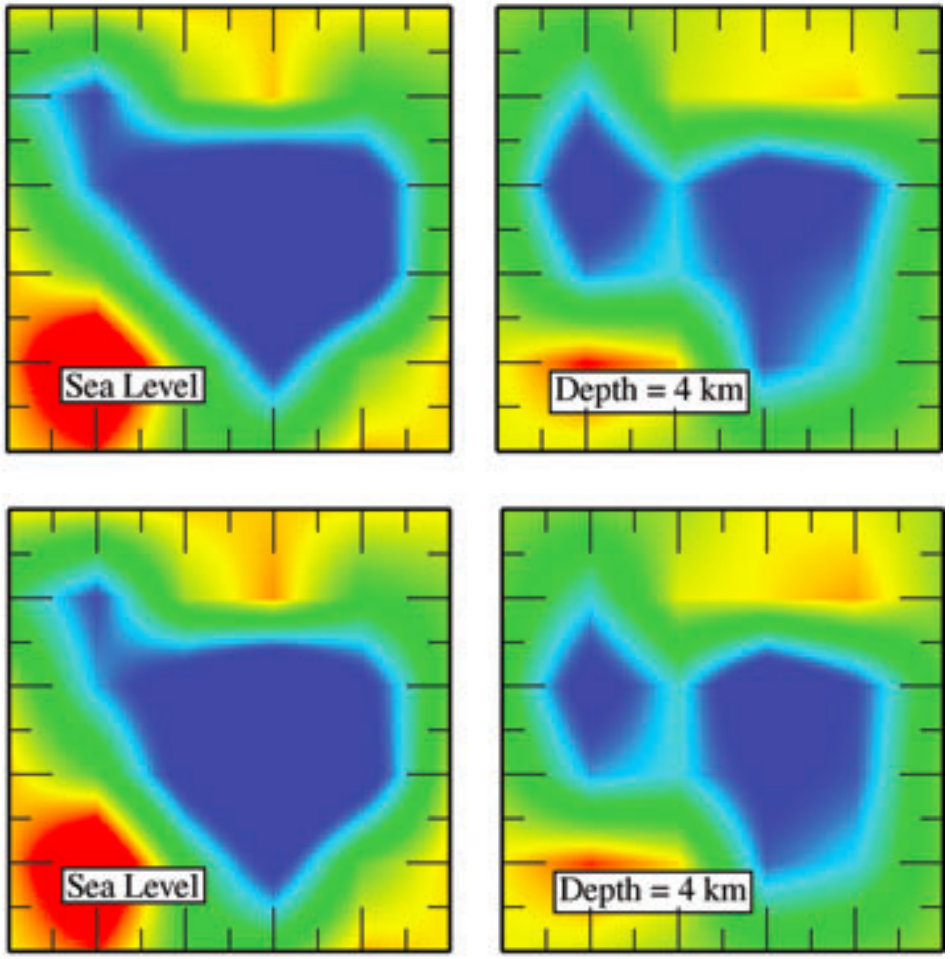

- Same theoretical models but with different ray distribution.
- Jointly Inverted models are different

Time-dependent seismic tomography

B. R. Julian[1] and G. R. Foulger[2]

Regularization in time

$$\phi(m_1, m_2, \cdots, m_n) = \sum_{i=1}^{n} \left\| G_i m_i - d_i \right\|_2^2 + \lambda_s^2 \sum_{i=1}^{n} \left\| D_s m_i \right\|_2^2 + \lambda_t^2 \sum_{i=1}^{n-1} \left\| D_t m_{i+1} - D_t m_i \right\|_2^2 ,$$

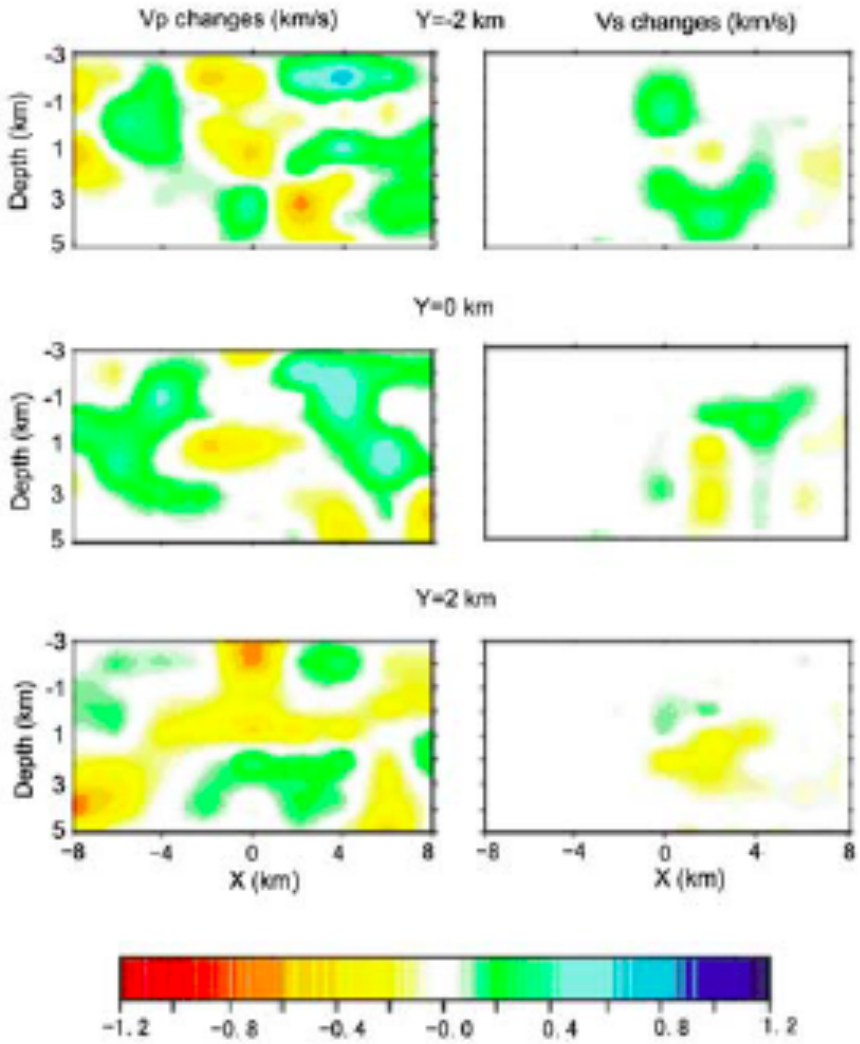
Vp changes (km/s)
Y=-2 km
Vs changes (km/s)
Depth (km)
-3
-1
1
3
5
Y=0 km
Y=2 km
-8
-4
0
4
8
X (km)
-1.2
-0.8
-0.4
-0.0
0.4
0.8
1.2

***Scattering*:**

Figure 3.7-9: Development of a *P*-wave coda.

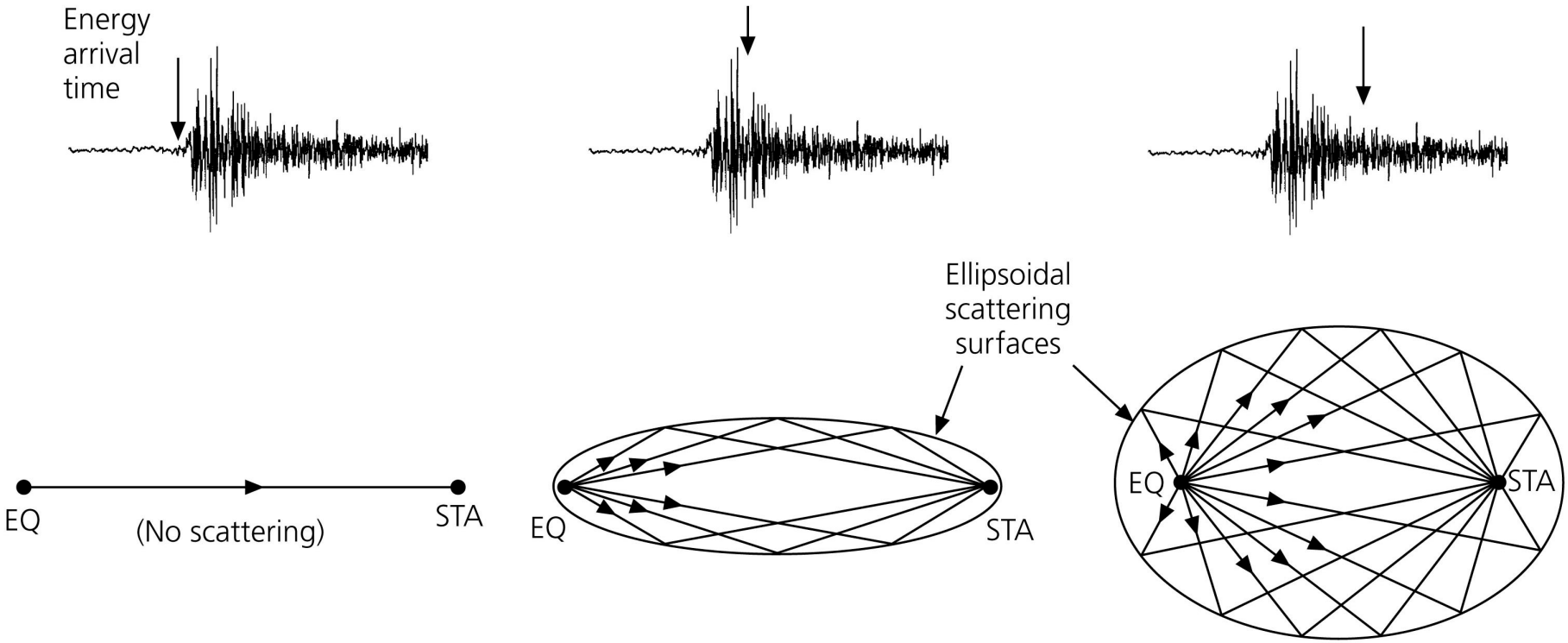

Scattering occurs when there are velocity heterogeneities in the medium with wavelengths on the order of λ of the wave.

A simulation of 100 randomly-perturbed scatterers…

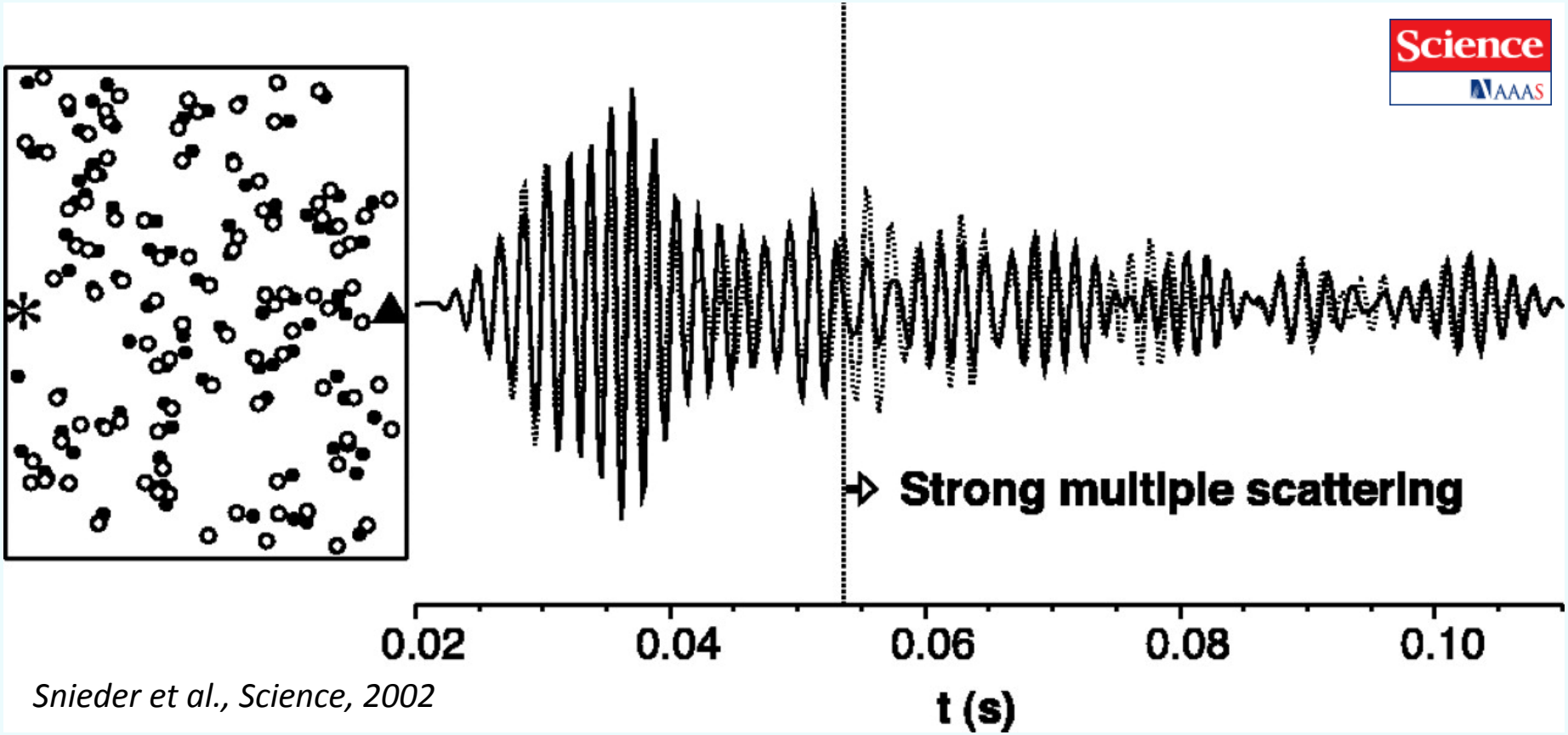

Snieder et al., Science, 2002

Moving the scatterers (here, 1/40th of the distance shown, so the perturbation is visible) mostly changes the shapes and amplitudes of the waveforms…

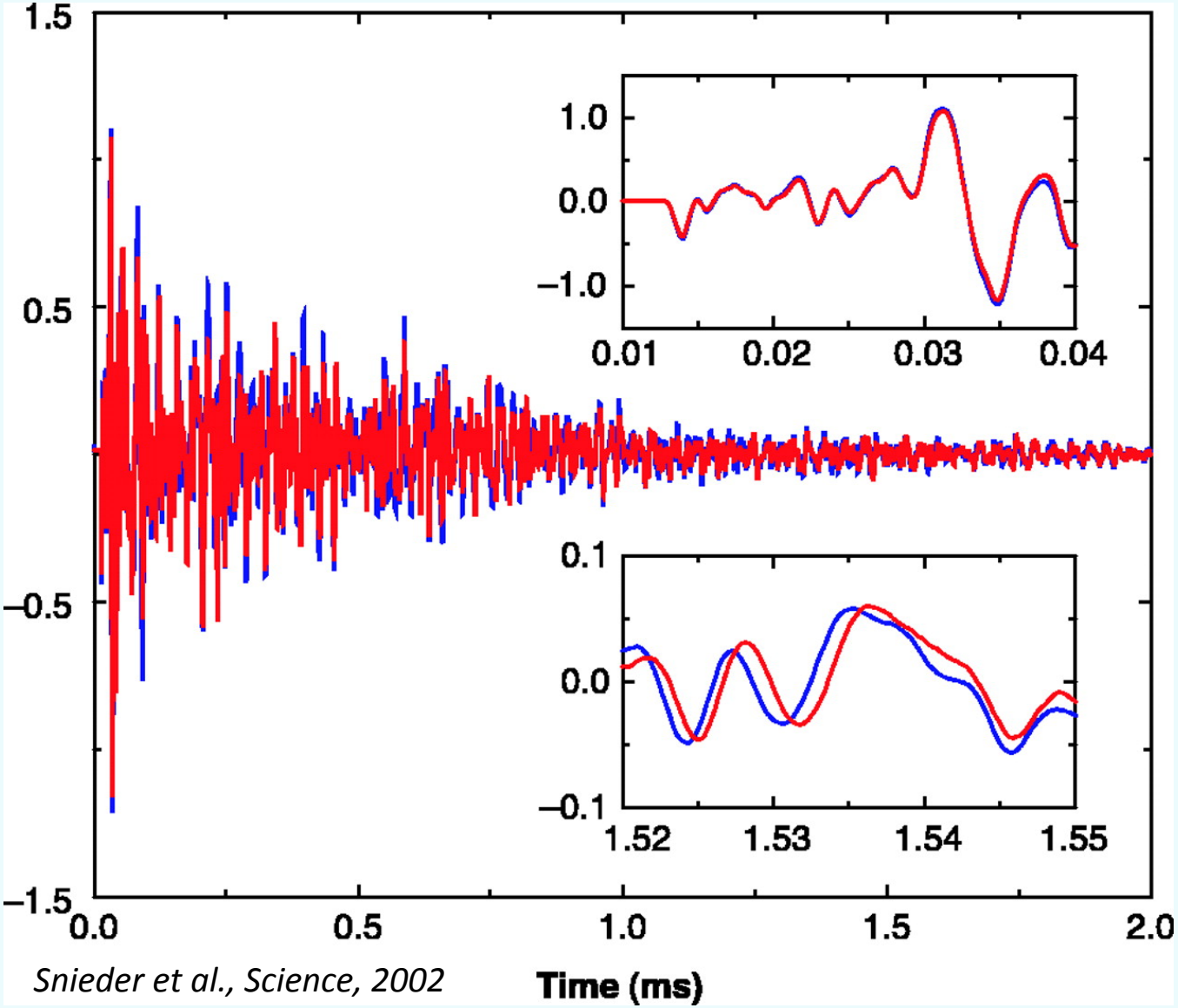

Snieder et al., Science, 2002

Waveforms measured in a granite sample at temperatures of 45°C (blue) and 50°C (red).

Changing the matrix velocity, by contrast, introduces a shift (delay or advance) that increases with coda time.

$$t_2 = t_1 + dt$$

$$v_2 = v_1 + dv$$

$$x = v_1 t_1 = v_2 t_2 = v_2(t_1 + dt)$$

$$dt = \frac{v_1 - v_2}{v_2} t_1 = \frac{-dv}{v_2} t_1$$

$$dt = \frac{d\eta}{\eta_1} t_1$$

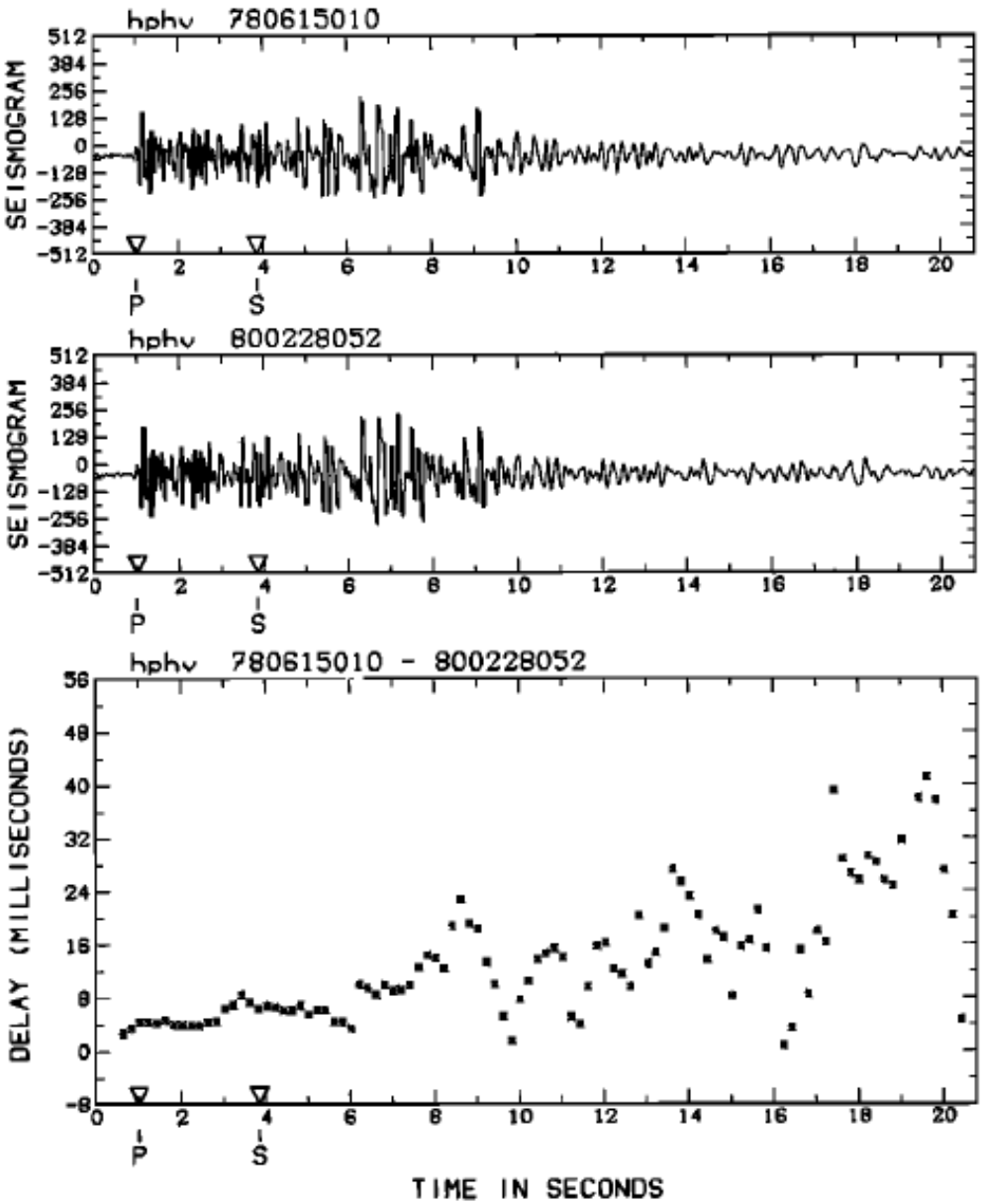

Poupinet et al. [1984]

Bulletin of the Seismological Society of America, Vol. 97, No. 1B, pp. 281–293, February 2007, doi: 10.1785/0120060120

Active Source Monitoring of Cross-Well Seismic Travel Time for Stress-Induced Changes

by Paul G. Silver, Thomas M. Daley, Fenglin Niu, and Ernest L. Majer

Near- and far-field effects of stress changes on cracks

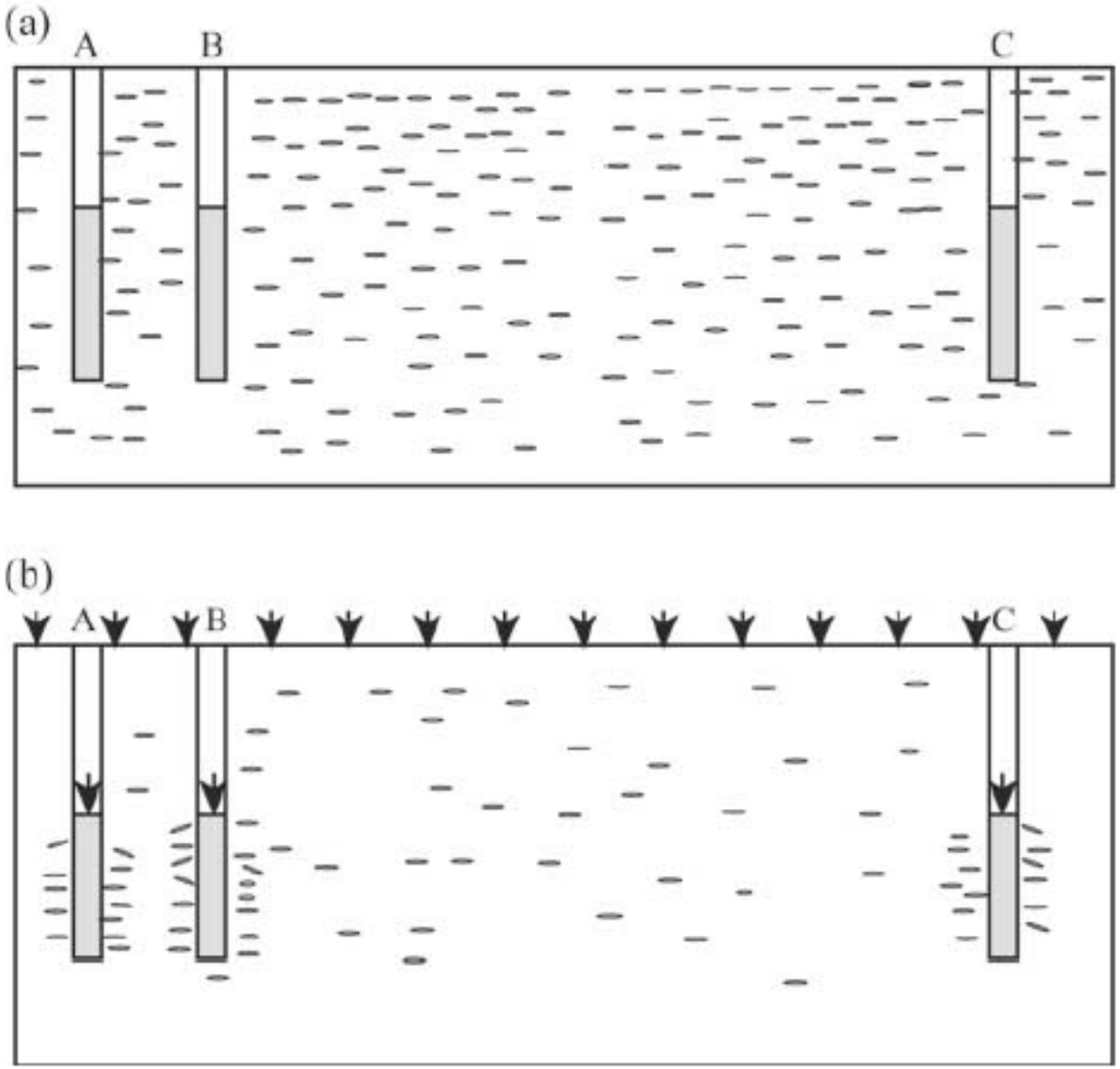

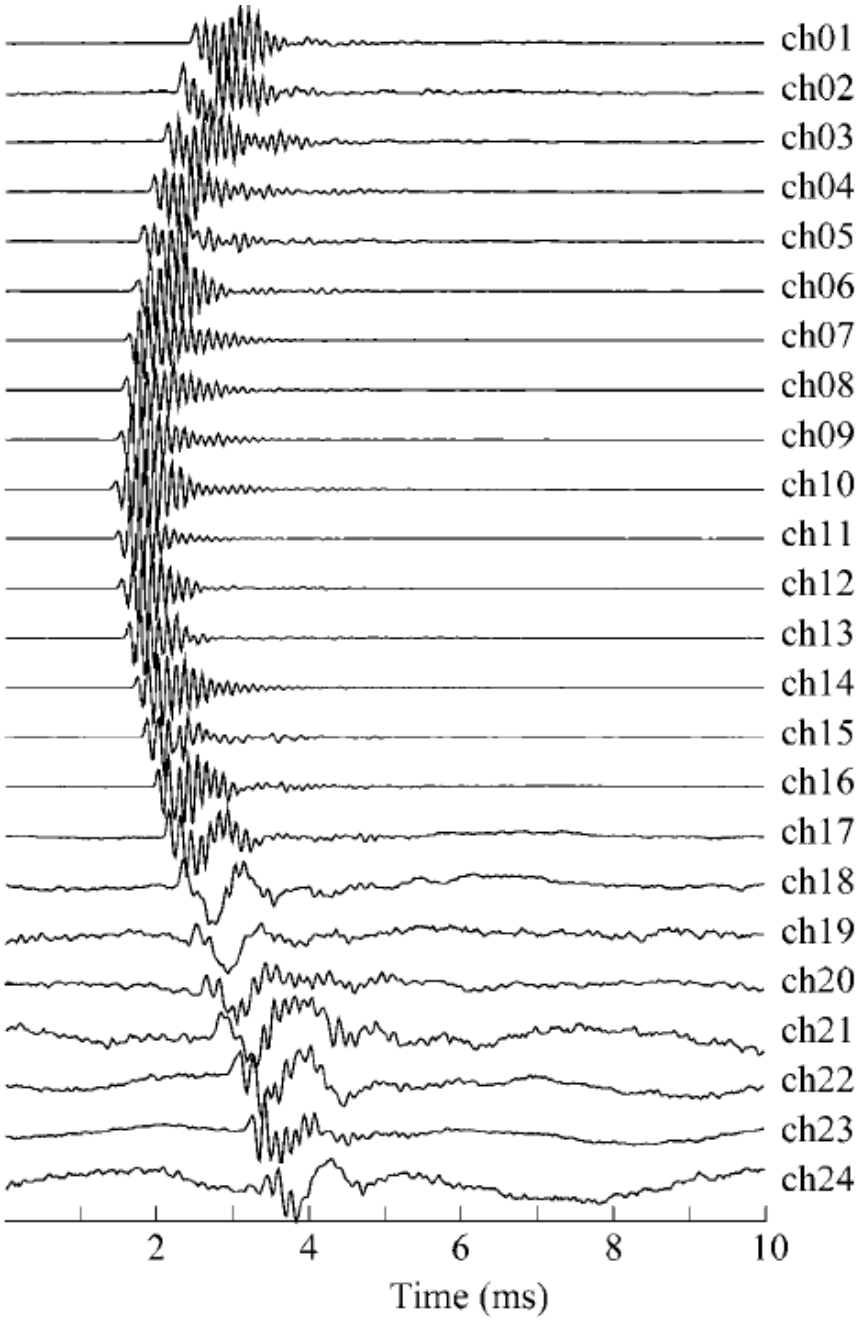

3-m separation between two wells

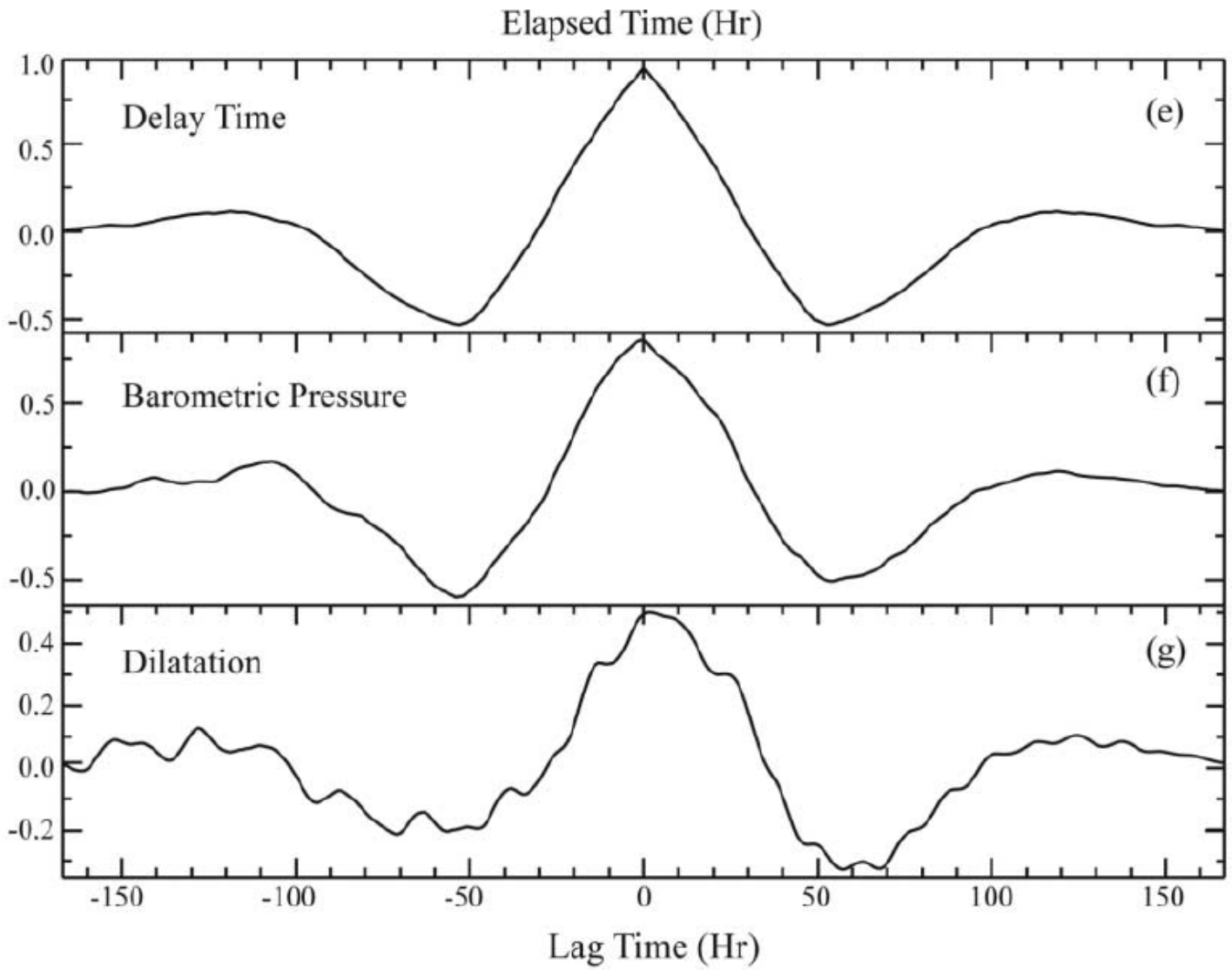
Elapsed Time (Hr)
Delay Time
(e)
Barometric Pressure
(f)
Dilatation
(g)
1.0
0.5
0.0
-0.5
0.5
0.0
-0.5
0.4
0.2
0.0
-0.2
-150
-100
-50
0
50
100
150
Lag Time (Hr)

Near- and far-field effects of stress changes on cracks

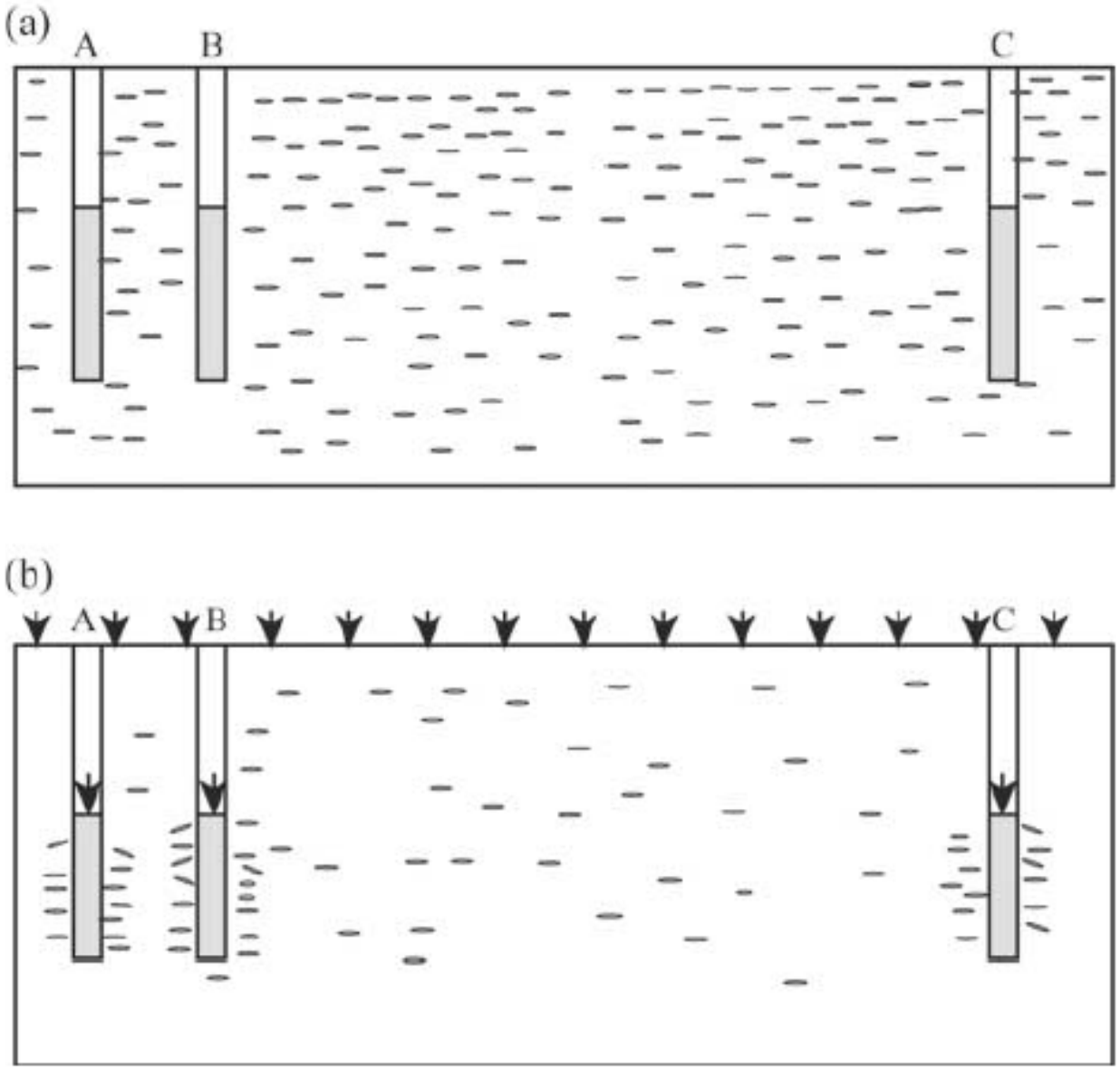

JOURNAL OF GEOPHYSICAL RESEARCH, VOL. 109, B10302, doi:10.1029/2004JB003011, 2004

Coseismic and postseismic velocity changes measured by repeating earthquakes

David P. Schaff[1] and Gregory C. Beroza

Department of Geophysics, Stanford University, Stanford, California, USA

Received 5 February 2004; revised 26 May 2004; accepted 20 July 2004; published 7 October 2004.

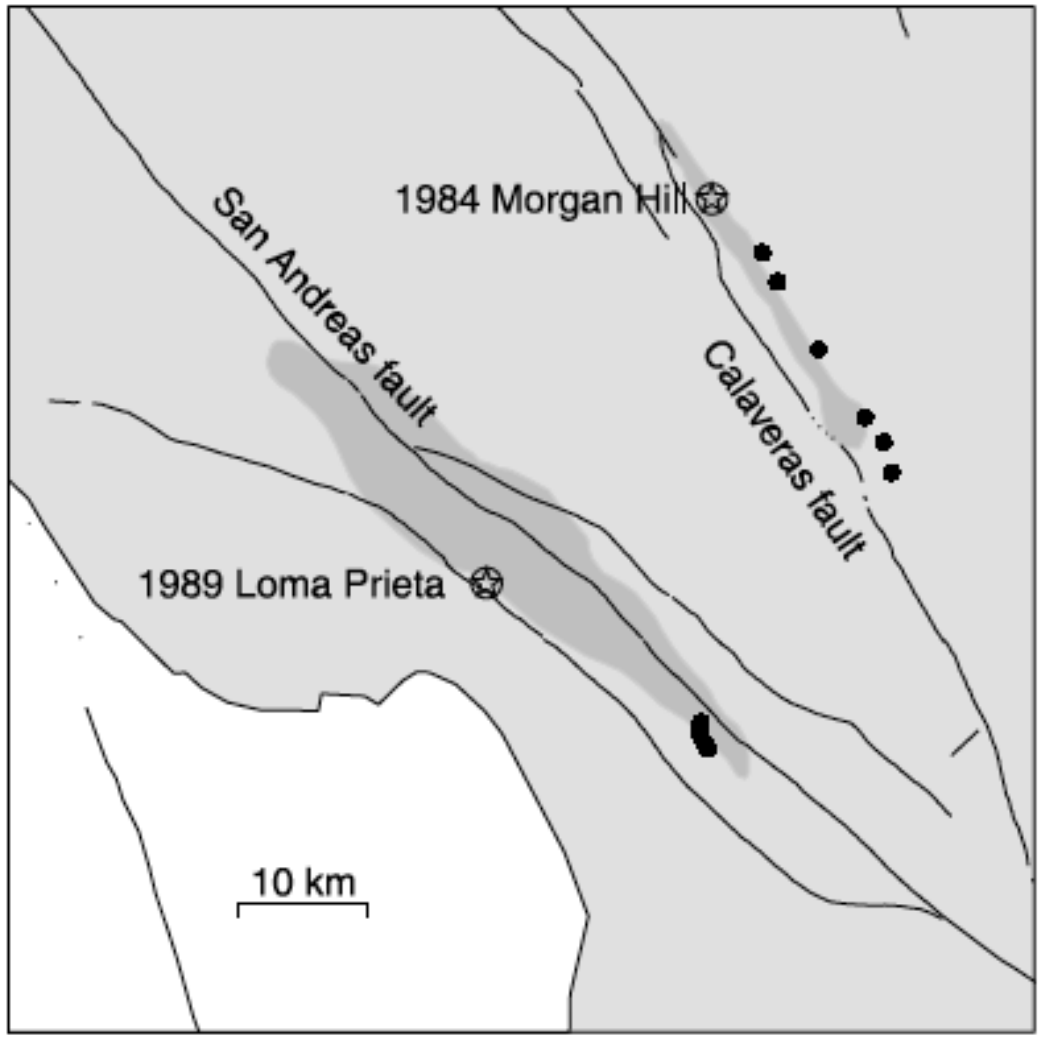

Figure 1. Multiplet clusters denoted by dots near the shaded aftershock zones of the 1984 Morgan Hill and 1989 Loma Prieta earthquakes.

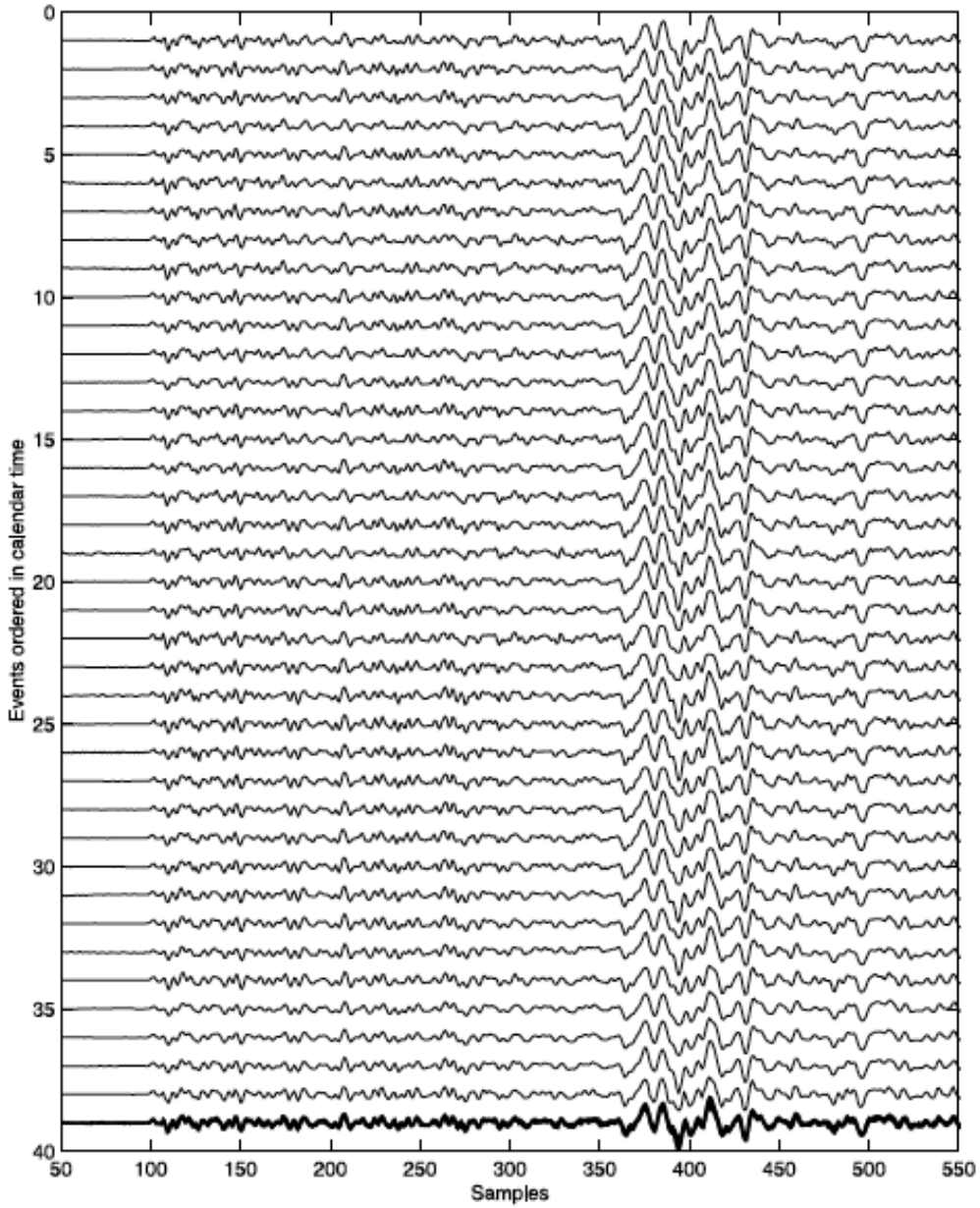

Repeating events
-with (almost) the same waveforms

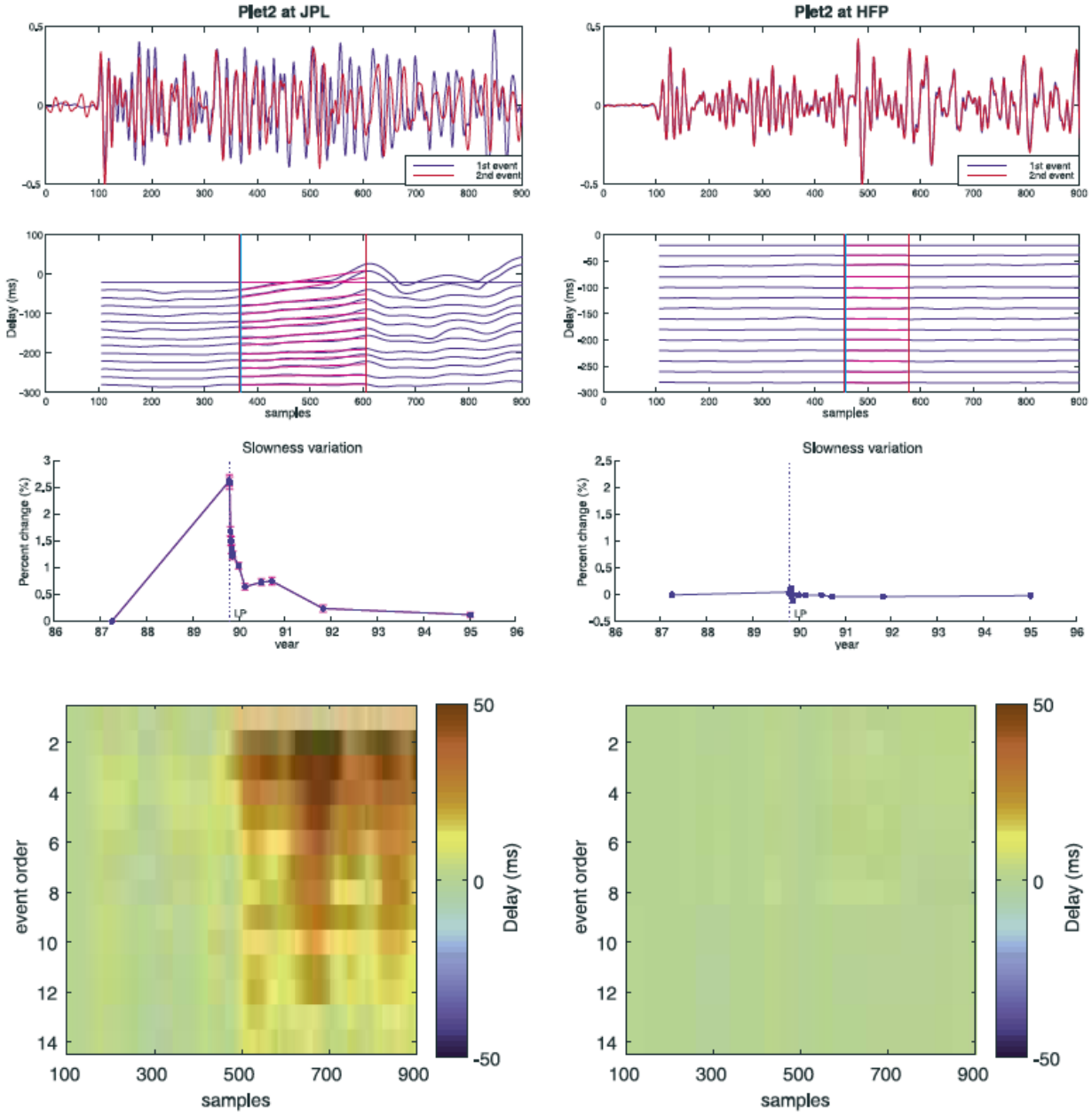

Figure 4. Comparison of (left) a station that does show velocity changes and (right) one that does not for plet2. See text for explanation.

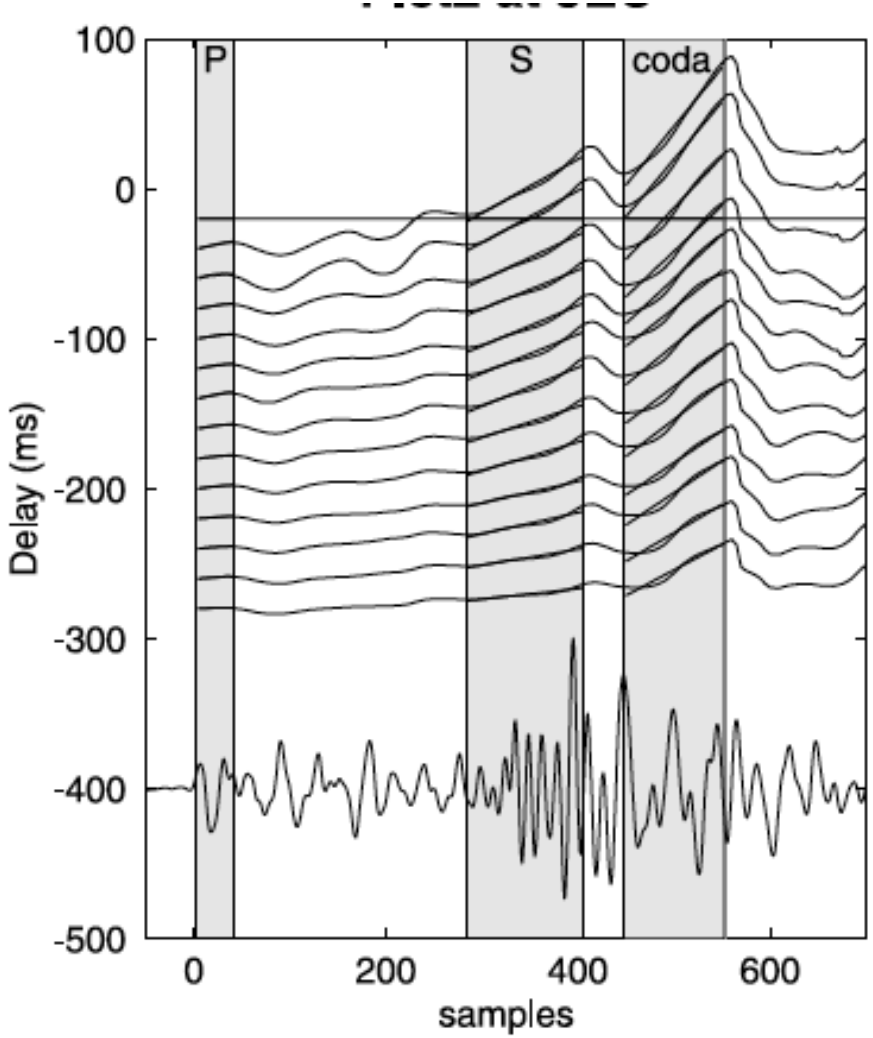
P
S
coda
100
0
-100
-200
-300
-400
-500
Delay (ms)
0
200
400
600
samples

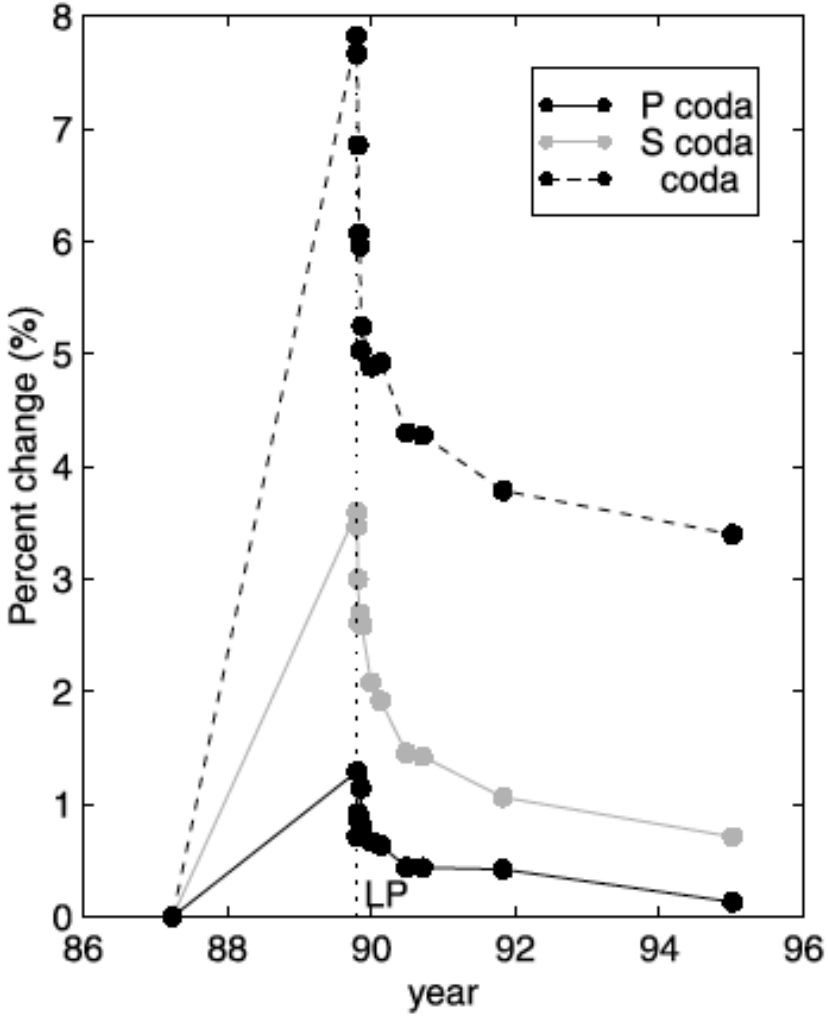
P coda
S coda
coda
LP
Percent change (%)
0
1
2
3
4
5
6
7
8
86
88
90
92
94
96
year

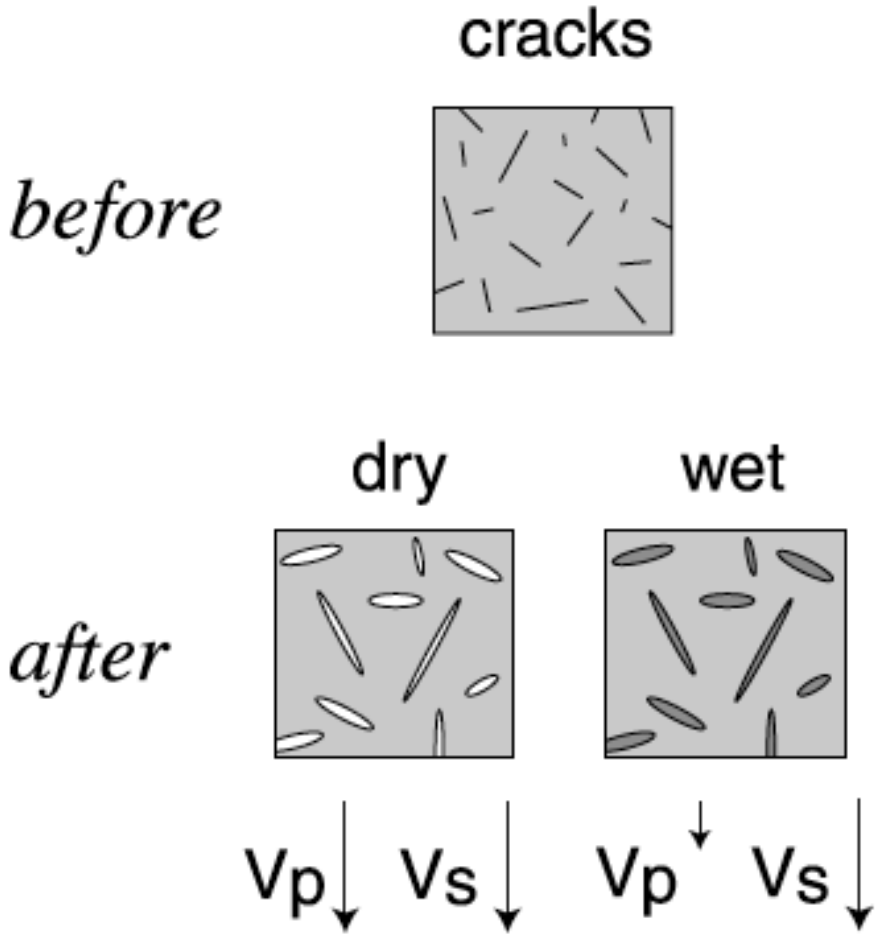

Figure 11. Cartoon demonstrating possible mechanism for observed differences in *P* and *S* wave velocity change behavior.

Seismic velocity imaging and monitoring of volcanic areas using ambient seismic noise

F. Brenguier (2008)

Virtual seismic source reconstruction

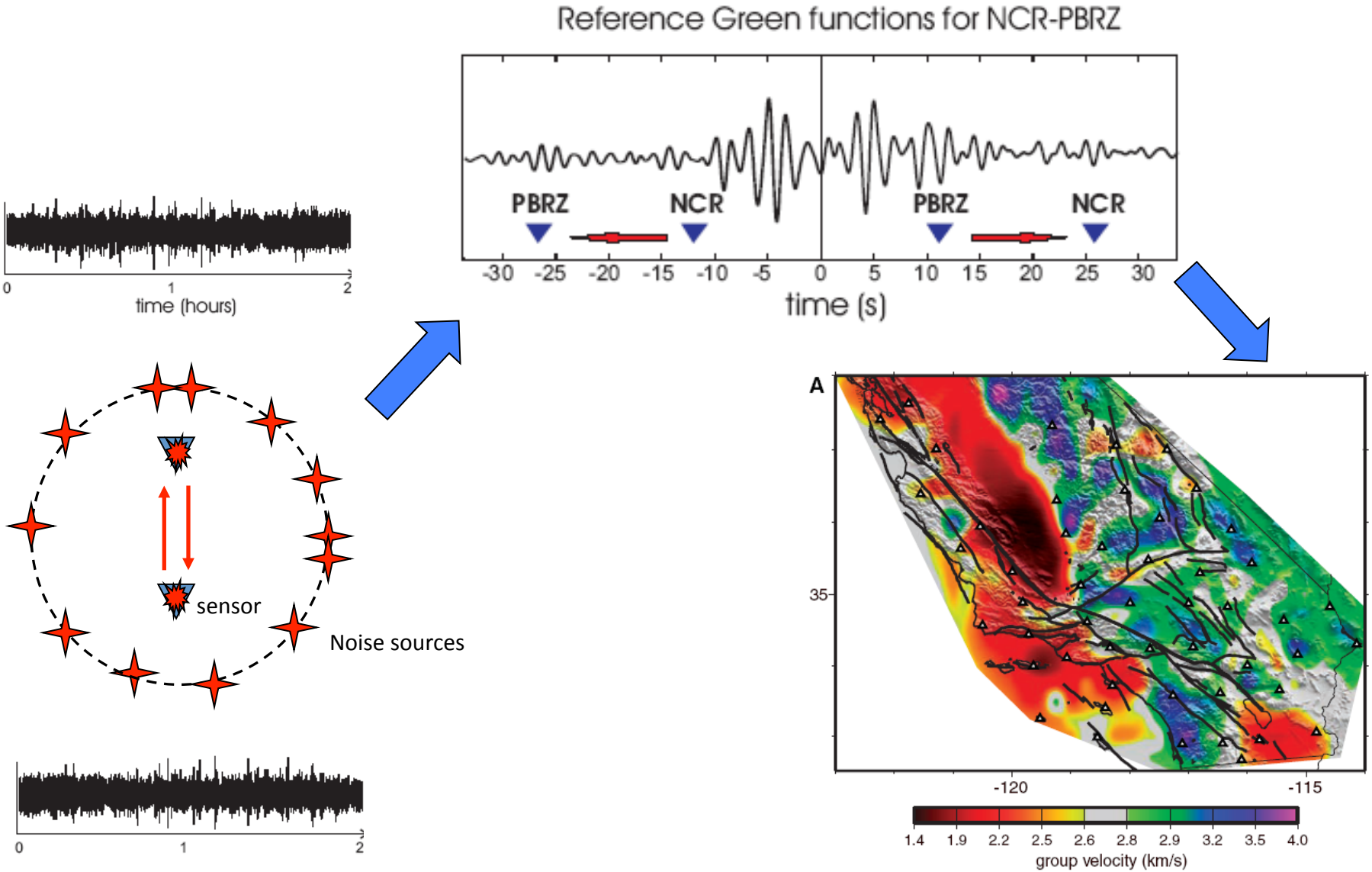

Shapiro et al. (2005)

A case study: Piton de la Fournaise volcano, La Réunion island

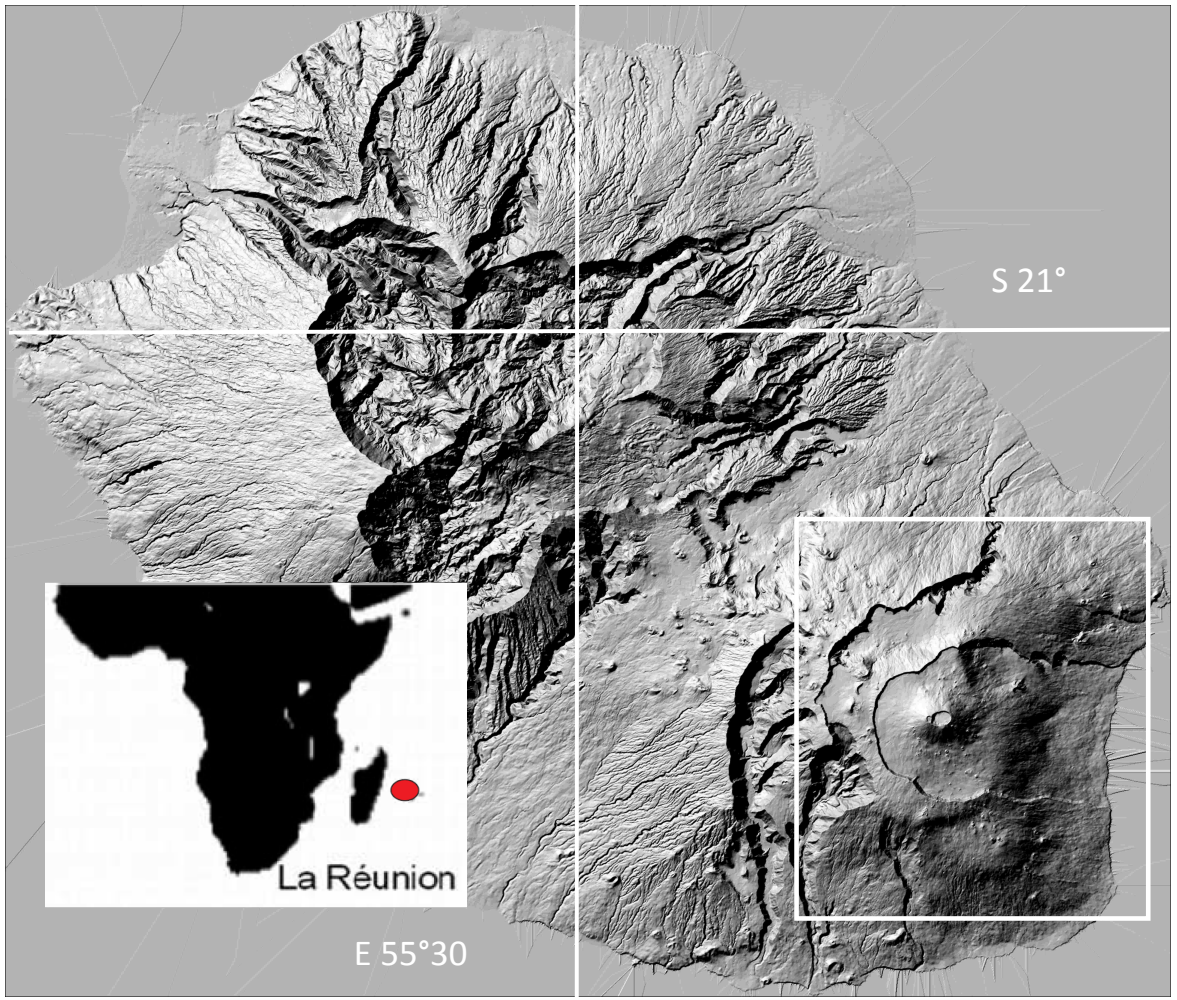

Temporal changes of seismic velocities using cross-correlations of seismic noise

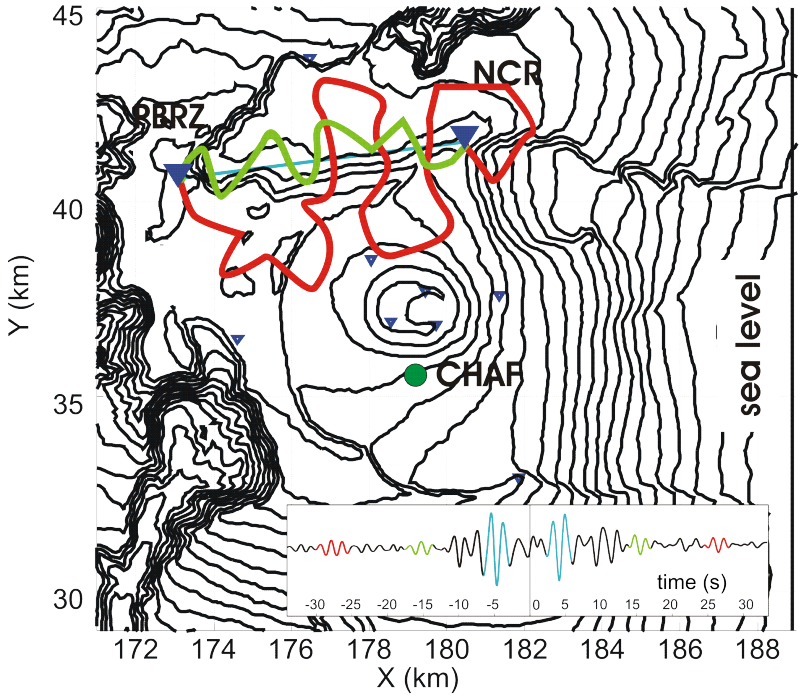

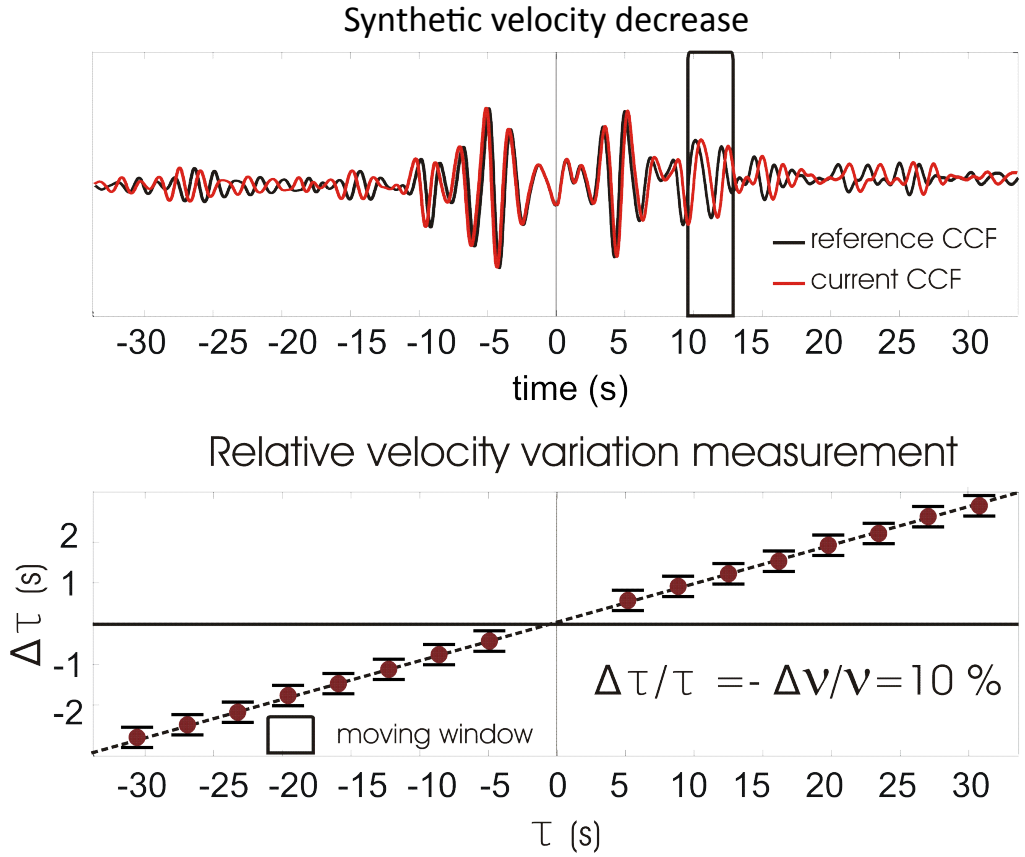

Velocity changes on Piton de la Fournaise

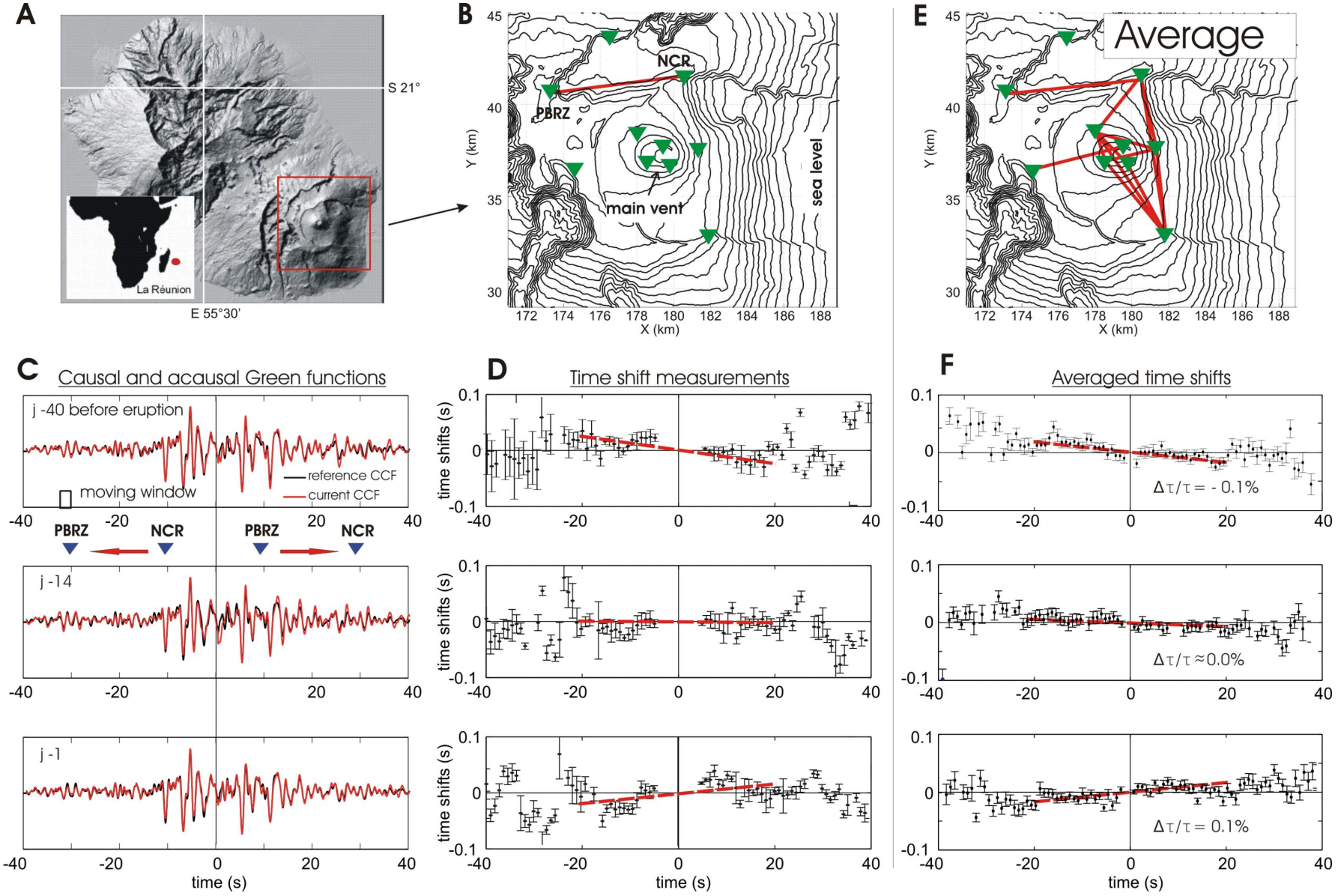

Velocity drops preceding eruptions

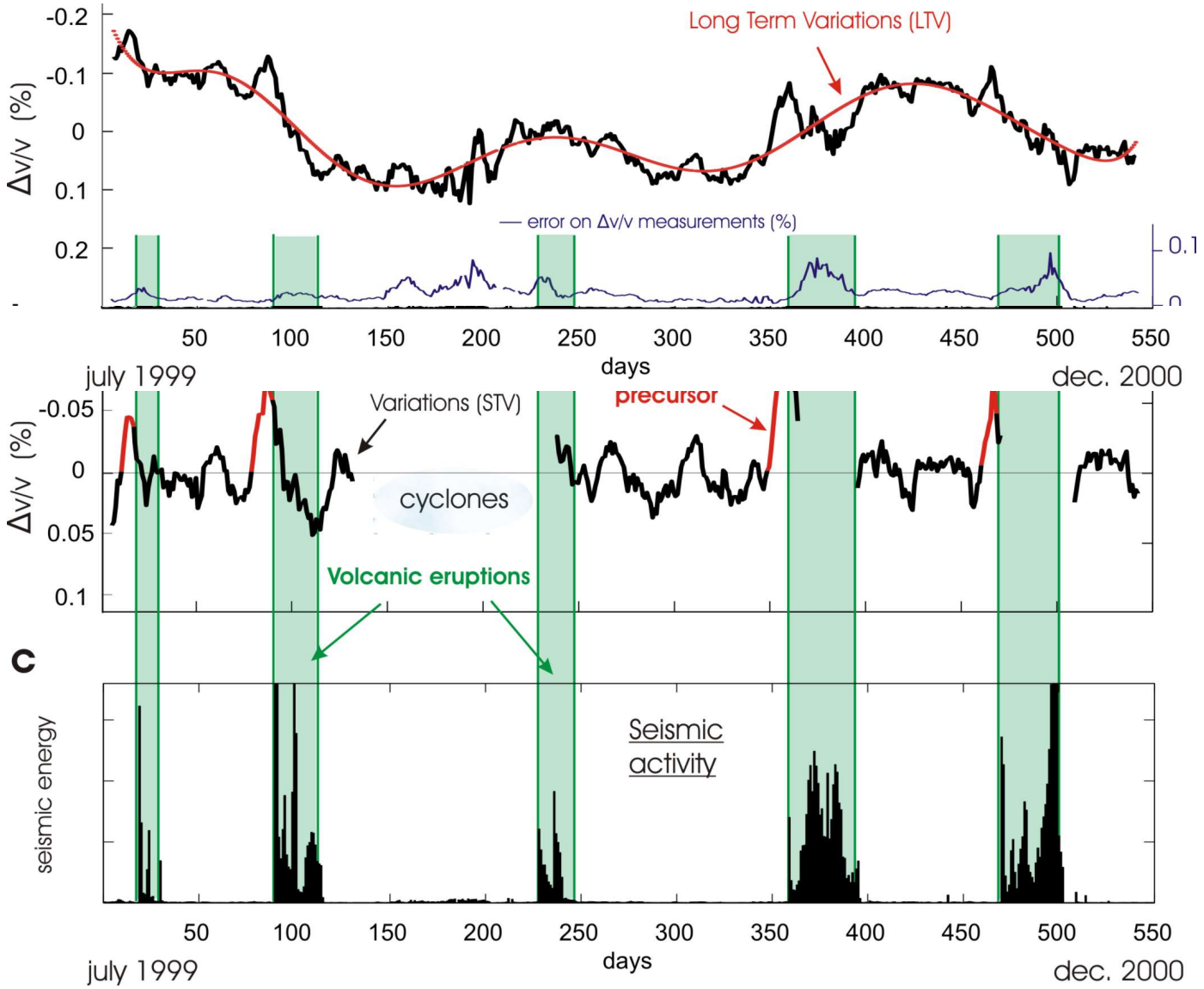

Brenguier et al., Nature Geoscience, 2008

Seismic velocity changes as a proxy for magma forcing

Seismic velocities are strongly sensitive to crack density.

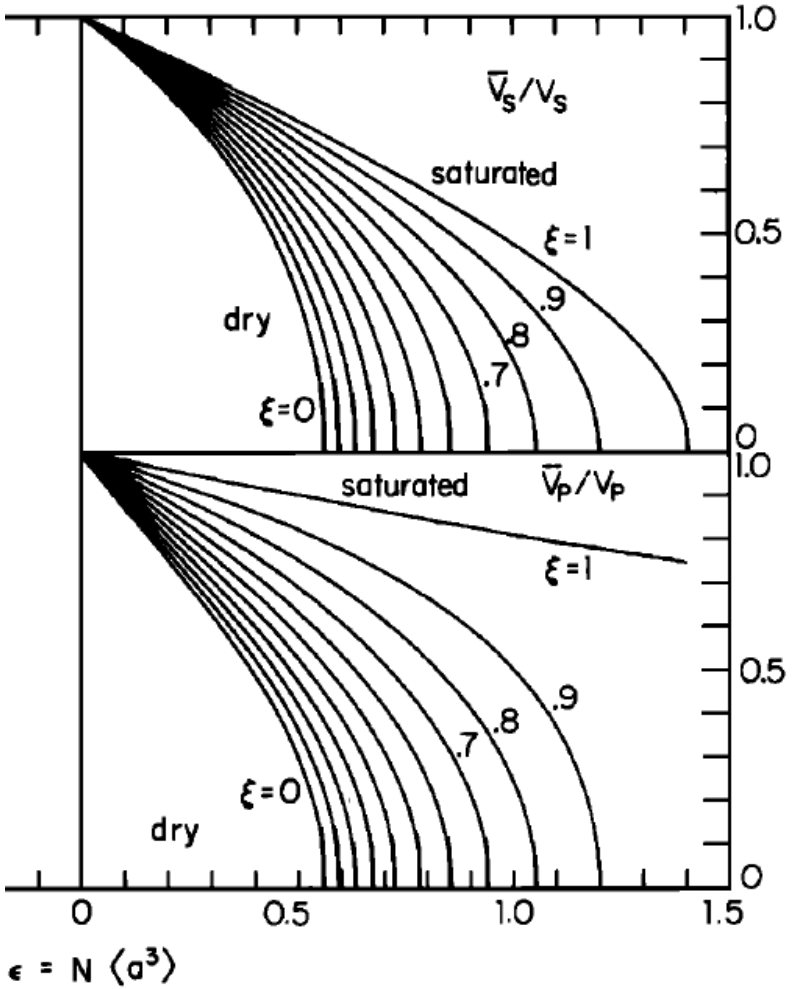

O'Connell, R. J., and B. Budiansky (1974), Seismic Velocities in Dry and Saturated Cracked Solids, J. Geophys. Res., 79(35), 5412–5426

Link between temporal changes and structure

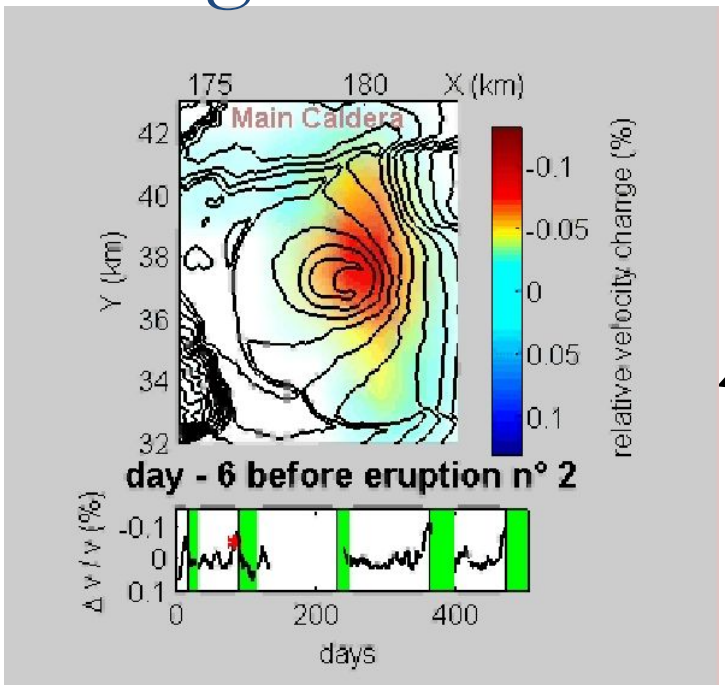

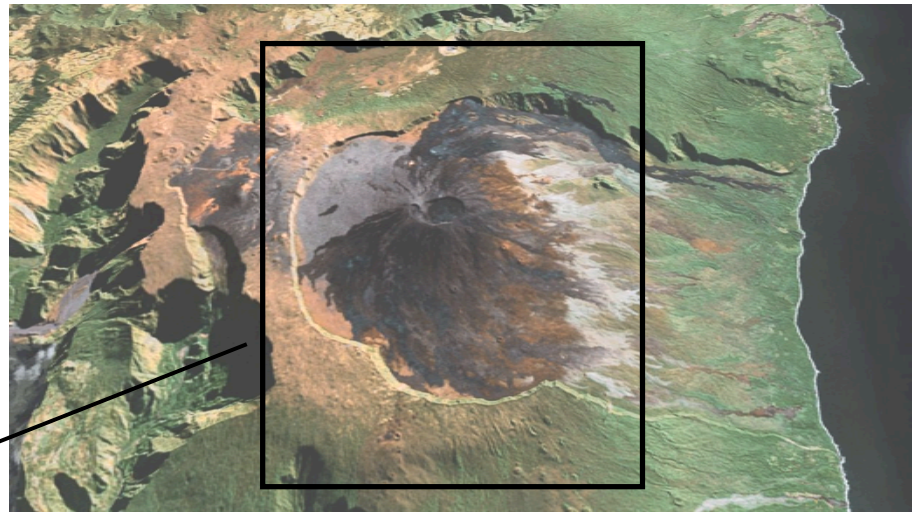

Magmatic intrusive complex

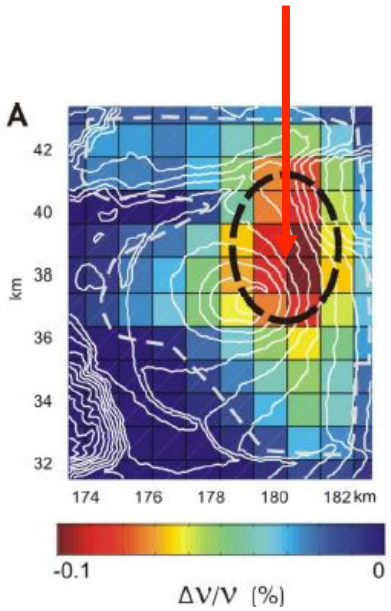

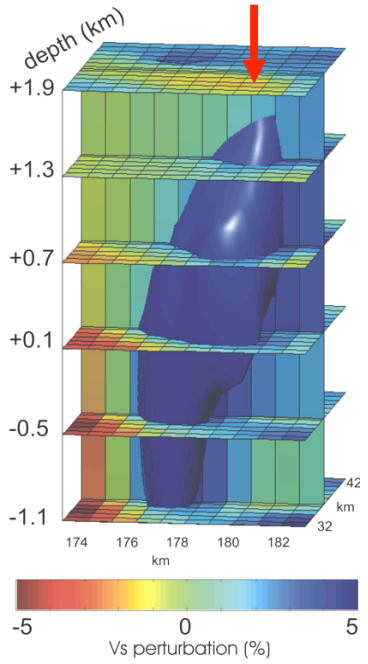

These velocity changes are linked to dilatation induced by stress changes